catalysts

MDPI

Review

Reactivity of Trapped and Accumulated Electrons in Titanium Dioxide Photocatalysis

Shigeru Kohtani *, Akira Kawashima and Hideto Miyabe

Department of Pharmacy, School of Pharmacy, Hyogo University of Health Sciences, 1-3-6 Minatojima, Chuo-ku, Kobe 650-8530, Japan; ak-kawashima@huhs.ac.jp (A.K.); miyabe@huhs.ac.jp (H.M.)

* Correspondence: kohtani@huhs.ac.jp; Tel.: +81-78-304-3158

Received: 20 September 2017; Accepted: 8 October 2017; Published: 13 October 2017

Abstract: Electrons, photogenerated in conduction bands (CB) and trapped in electron trap defects (Ti_{ds}) in titanium dioxide (TiO_2), play crucial roles in characteristic reductive reactions. This review summarizes the recent progress in the research on electron transfer in photo-excited TiO_2. Particularly, the reactivity of electrons accumulated in CB and trapped at Ti_{ds} on TiO_2 is highlighted in the reduction of molecular oxygen and molecular nitrogen, and the hydrogenation and dehalogenation of organic substrates. Finally, the prospects for developing highly active TiO_2 photocatalysts are discussed.

Keywords: titanium dioxide; photocatalysis; surface defects; bulk defects; trapped electrons; accumulated electrons

1. Introduction

Since Fujishima and Honda discovered photoelectrochemical water splitting on titanium dioxide (TiO_2) photoelectrodes in the early 1970s [1], TiO_2 photocatalysis has been applied in various fields, such as the storage of solar energy [2–5], environmental purification [6], organic synthesis [7–11], anti-bacterial applications [12], and anti-fogging treatments [12,13]. These characteristic photo-functionalities are induced by incident light, in which the behavior of photogenerated electrons and holes, as well as the roles of defects formed on surface and in lattice, are of particular importance. The defect sites are the recombination centers for the photogenerated electrons and holes, because photocatalytic activities decrease with increasing the amount of defects created [2,6,8]. However, Amano et al. reported that the introduction of defect states in TiO_2 with H_2 reduction treatment greatly enhanced the photocatalytic activity for the water oxidation reaction in aqueous solution [14,15]. Moreover, Kong and coworkers claimed that tuning the relative concentration ratio of bulk defects/surface defects in TiO_2 nanocrystal improves the separation efficiencies of photogenerated electrons and holes, thereby enhancing the photocatalytic activity [16]. Thus, further understanding of the defects in TiO_2 necessitates the development of highly active photocatalysts.

The properties of defects—such as energy levels, structures, and interactions with adsorbates—have been reviewed by Diebold [17], Henderson [18], and Nowotny [19,20] in detail, but many unanswered questions remain. Recent studies in this field have made the considerable progress during the last decade. This review summarizes the recent progress in the research on the defects in TiO_2. Herein, we focus on the properties of electron trap defects formed within the bandgap of TiO_2 associated with Ti defects, specifically the intra-bandgap Ti states (Ti_{ds}). Firstly, the fate of photogenerated electron and holes in TiO_2 are described with respect to Ti_{ds} and hole trap sites in Section 2. Next, the origin of Ti_{ds} and their energy distribution in TiO_2 are considered in Section 3. In Section 4, the reactivity of electrons trapped at Ti_{ds} and accumulated in the conduction band (CB) on the representative reductive reactions are highlighted. Finally, the prospect for developing a highly active TiO_2 catalyst is discussed.

2. Fate of Photogenerated Electrons and Holes in TiO_2

Although several models exist for the charge transport, trapping, and the reaction of photogenerated electrons and holes on photoexcited TiO_2, we adopted a schematic model for the anatase TiO_2 based on the recent selected reviews and reports as illustrated in Figure 1 [11,21–25].

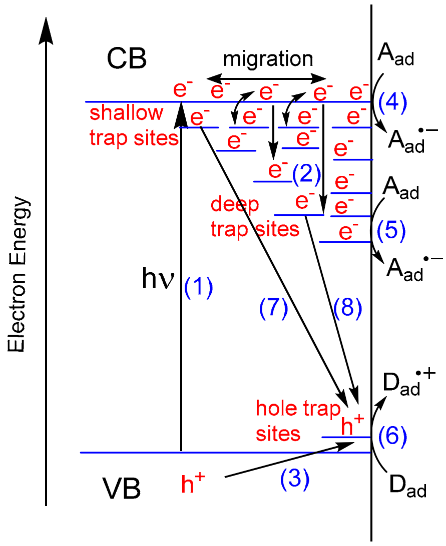

Figure 1. Schematic model of the earlier stage of photocatalysis in the anatase titanium dioxide (TiO_2). CB: conduction band; VB: valence band; A_{ad}: adsorbed electron acceptor; D_{ad}: adsorbed electron donor.

This model consists of several steps:

Step 1. Electron–hole pair generation

$$TiO_2 + h\nu \rightarrow TiO_2\ (e^- + h^+) \qquad ([<100\ fs])$$

Step 2. Trapping CB electrons (e_{cb}^-) at defect Ti^{4+} sites

$$Ti_{ds}^{4+} + e_{cb}^- \rightarrow Ti_{ds}^{3+} \qquad ([100\ fs\text{–}500\ ps])$$

Step 3. Trapping valence band holes (h_{vb}^+) at terminal Ti–OH or surface Ti–O–Ti sites

$$Ti\text{-}O_sH \text{ or } Ti\text{-}O_s\text{-}Ti + h_{vb}^+ \rightarrow Ti\text{-}O_sH^{\cdot+} \text{ or } Ti\text{-}O_s^{\cdot+}-Ti \qquad ([<100\ fs\text{–}200\ fs])$$

Step 4. Reduction of adsorbed electron acceptor (A_{ad}) with e_{cb}^- at reduction sites

$$e_{cb}^- + A_{ad} \rightarrow A_{ad}^{\cdot-} \qquad ([>10\ ns])$$

Step 5. Reduction of A_{ad} with electrons trapped at defect sites (Ti_{ds}^{3+})

$$Ti_{ds}^{3+} + A_{ad} \rightarrow Ti_{ds}^{4+} + A_{ad}^{\cdot-} \qquad ([\text{slow process}])$$

Step 6. Oxidation of adsorbed electron donor (D_{ad}) by trapped holes at oxidation sites

$$Ti\text{-}O_sH^{\cdot+} \text{ or } Ti\text{-}O_s^{\cdot+}\text{-}Ti + D_{ad} \rightarrow Ti\text{-}O_sH \text{ or } Ti\text{-}O_s\text{-}Ti + D_{ad}^{\cdot+} \qquad ([100\ ps\text{–}10\ ns])$$

Step 7. Recombination of e_{cb}^{-} with trapped holes

$$e_{cb}^{-} + \text{Ti-O}_s\text{H}^{\cdot +} \text{ or } \text{Ti-O}_s^{\cdot +}\text{-Ti} \rightarrow \text{Ti-O}_s\text{H or Ti-O}_s\text{-Ti} \qquad ([1\text{–}10\text{ ps}])$$

Step 8. Recombination of Ti_{ds}^{3+} with trapped holes

$$\text{Ti}_{ds}^{3+} + \text{Ti-O}_s\text{H}^{\cdot +} \text{ or } \text{Ti-O}_s^{\cdot +}\text{-Ti} \rightarrow \text{Ti}_{dt}^{4+} + \text{Ti-O}_s\text{H or Ti-O}_s\text{-Ti} \qquad ([>20\text{ ns}])$$

where time scales for each step are described in brackets [21–24]. The time scales depend on the crystalline phases, crystallinity, specific surface area, and the presence of bulk and surface defect states in TiO_2. The following assumptions were applied to this model: (a) CB electrons (e_{cb}^{-}) contain both electrons in CB and electrons trapped at shallow sites, located just below the CB edge of TiO_2 within 0–0.05 eV. These electrons were assumed to be in thermal equilibrium in the bulk CB and at the shallow trap sites; (b) Valence band holes (h_{vb}^{+}) are rapidly transported to the surface hole trap sites ($\text{Ti–O}_s\text{H}$ or $\text{Ti–O}_s\text{–Ti}$) (Step 3); (c) trapped holes ($\text{Ti–O}_s\text{H}^{\cdot +}$ or $\text{Ti–O}_s^{\cdot +}\text{–Ti}$) are the main oxidants for the adsorbed electron donor (D_{ad}) (Step 6); and (d) charge carrier recombination occurs between e_{cb}^{-} and holes trapped at the surface trap sites (Step 7), as well as between electrons trapped at Ti defect states (Ti_{ds}^{3+}) and holes trapped at the surface trap sites (Step 8), whereas the interband electron–hole carrier recombination ($e^{-} + h^{+} \rightarrow h\nu$ or heat) is negligible.

These assumptions can be justified as follows. Tamaki and coworkers described the charge carrier dynamics under weak excitation conditions for nano-crystalline anatase TiO_2 samples in femtosecond to microsecond time scales [22,23], which should be compatible with the actual photocatalytic reactions under the usual UV irradiation conditions. They observed the e_{cb}^{-} and h_{vb}^{+} pair generation within 100 fs, and the e_{cb}^{-} migration between CB and shallow trap sites in equilibrium. These electrons then relaxed to deep trap sites (Ti_{ds}) with an approximate 500 ps time constant. Meanwhile, h_{vb}^{+} was rapidly trapped to the surface terminal $\text{Ti–O}_s\text{H}$ sites within 100 fs to create $\text{Ti–O}_s\text{H}^{\cdot +}$ [22,23]. If the photoinduced event occurred in alcohols, the lifetime of the $\text{Ti–O}_s\text{H}^{\cdot +}$ generated on the TiO_2 surface would be in the nanosecond or sub-nanosecond time scale (approximately 0.1–3 ns in alcohols) due to the fast reaction of $\text{Ti–O}_s\text{H}^{\cdot +}$ with the abundant alcohol adsorbed on the TiO_2 surface [24]. Therefore, the free h_{vb}^{+} rarely presents in the bulk or on the surface of TiO_2, so that e_{cb}^{-} may recombine only with the trapped holes.

3. Origin and Energy Distribution of Electron Trap Defects (Ti_{ds})

The bulk and surface Ti_{ds} are formed in reduced or doped TiO_2 in both rutile and anatase phases [17–20]. As depicted in Diebold's review [17], the bulk Ti_{ds} are easily created in the rutile single crystal by thermal annealing in a vacuum, resulting in the formation of blue color centers, indicating high conductivity. Therefore, TiO_2 is classified as an n-type semiconductor. The H_2 reduction of TiO_2 creates both oxygen vacancies and Ti^{3+} ions, which is an electron trapped in a Ti^{4+} lattice site, as described in Reaction (1) using Kröger–Vink notation [14,15,19,20]

$$O_O^x + 2Ti_{Ti}^x + H_2 \rightarrow V_O^{\bullet\bullet} + 2Ti\prime_{Ti} + H_2O \tag{1}$$

where O_O^x is an O^{2-} ion in the oxygen lattice site, $V_O^{\bullet\bullet}$ is an oxygen vacancy with a double positive charge, and Ti'_{Ti} is a Ti^{3+} ion in the titanium lattice site. The two Ti'_{Ti} that are created per $V_O^{\bullet\bullet}$ have two excess electrons, which are responsible for the n-type conductivity, the blue-black colorization, and the enhancement of photocatalytic activity on TiO_2. The H_2 reduction on TiO_2 can also induce a disordered structure in the surface layer of TiO_2 nanocrystals, indicated by black TiO_2 [26–28]. Black TiO_2 exhibits high photocatalytic performance in decomposing organic pollutants and in generating hydrogen gas in an aqueous methanol solution under solar light irradiation. The other titanium oxides that have Ti_{ds} are the F-doped or Nb-doped TiO_2, in which oxygen atoms are substituted with fluorine atoms or Ti atoms are replaced with Nb atoms, respectively [29]. Another type of Ti defect in TiO_2

is titanium interstitials ($Ti_i^{\bullet\bullet\bullet}$) possessing excess Ti atoms or ions in the lattice or in the near-surface region on TiO_2 surface [17–20,30].

Facile laser ablation and processing techniques have been developed to introduce the defects into TiO_2 nanocrystals and colloids in liquid [31–34]. In a typical procedure, TiO_2 suspensions are irradiated by a high-intensity pulsed laser with frequent repetition rates to produce the characteristic blue-black TiO_2. The obtained TiO_2 nanoparticles enhanced the photocatalytic activities in decomposing an organic dye [31] and in a water splitting reaction [32].

The electronic energy of Ti_{ds} is located just below the CB edge in the band gap of TiO_2 in a broad range of 0–1.8 eV [35]. Di Valentin and co-workers theoretically calculated the energy levels of point defects in bulk anatase TiO_2, which are located at 0.3, 0.4, 0.7, and 0.8 eV below the CB edge, for six-fold-coordinated Ti introduced by F- or Nb-doping, Ti–OH species associated with hydrogen doping, five-coordinated Ti'_{Ti} associated with the oxygen vacancy site, and titanium interstitials $Ti_i^{\bullet\bullet\bullet}$, respectively [29]. Deskins et al. calculated the relative energies of Ti_{ds} formed in the {110}-terminated rutile TiO_2 surface by means of the density functional theory (DFT), known as the DFT + U method [36,37]. They modeled the formation of Ti_{ds} at various Ti sites, such as the five-coordinated Ti and oxygen vacancies [37]. The calculation for the five-coordinated Ti in the presence of surface hydroxyls indicated that deep Ti_{ds} sites may exist in the second Ti layer from the surface or under the five-coordinated Ti rows [36].

The presence of these Ti_{ds} species, such as Ti'_{Ti} and $Ti_i^{\bullet\bullet\bullet}$, can be experimentally confirmed by means of electron spin resonance (ESR) [38–42], infrared radiation (IR) [40,42–48], ultraviolet-visible absorption (UV–vis) [14,42,49–51], photoluminescence (PL) [52], photoacoustic [53–56], and photoelectron spectroscopies [17,18,30]. Scanning tunneling microscopy (STM) and atomic force microscopy (AFM) are powerful tools for the direct observation of surface Ti_{ds} [17,18,30,57–59]. The oxygen vacancy (Ti'_{Ti} accompanied by $V_O^{\bullet\bullet}$) [57–59] and interstitial Ti ($Ti_i^{\bullet\bullet\bullet}$) [30] sites were directly observed on the TiO_2 surface.

The Ti_{ds} described above are not the only type of point defects. There are many types of lattice defects including step edges, line defects, grain boundaries, and impurities [17]. The Ti_{ds} energies can be strongly affected by site heterogeneity due to the local structures. Furthermore, under actual photocatalytic conditions, the TiO_2 surface is always covered by adsorbates, especially solvent molecules; thus, the energy of Ti_{ds} should depend on the adsorbed species [19,20]. Therefore, the information from the theoretical calculations and the photoelectron spectroscopy, applied to the clean catalyst surfaces under ultra-high vacuum conditions, may be limited for actual photocatalytic systems. To address this issue, Ohtani et al. developed a powerful tool for measuring the energy-resolved distribution of electron trap states for many types of TiO_2 powders, composed of anatase, rutile, and brookite in methanol-containing gas phase, by means of reversed double-beam photoacoustic spectroscopy (RDB-PAS) [56]. They showed that the electron energy of the trap states is distributed around the CB edge of TiO_2 and the distribution range of anatase TiO_2 is relatively broader than that of rutile TiO_2 (Figure 2). The energy distribution patterns for both anatase and rutile TiO_2 powders are similar to those obtained by the photochemical method, which uses the surface reaction of the trapped electrons with methyl viologen to release its cation radical in de-aerated aqueous solution containing methanol as a sacrificial reagent [60]. They also revealed that the total density of the traps is well-correlated to the specific surface area of TiO_2 powders, suggesting that the electron trap sites are predominantly located on the surface of TiO_2, and they do not depend on the type of crystallites in anatase, rutile, or their mixtures.

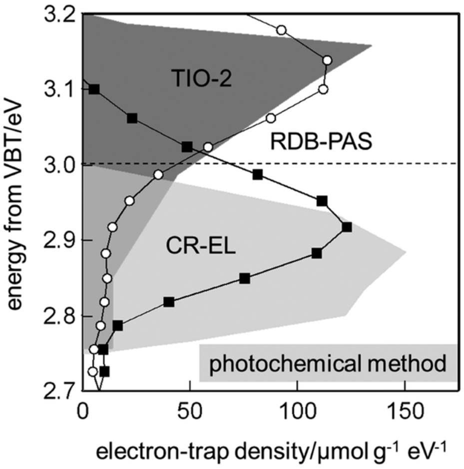

Figure 2. Comparison of energy-resolved distribution of electron traps (ERDT) patterns measured using the photochemical method shown by the grey patterns [60], and reversed double-beam photoacoustic spectroscopy (RDB-PAS), shown by the plots [56], for representative anatase (TIO^{-2}; 18 m^{2}g^{-1}) and rutile (7 m^{2}g^{-1}) samples. The top line, at 3.2 eV, and the dashed line show the conduction bands (CB) edge positions of anatase and rutile estimated by the reported bandgaps at 3.2 and 3.0 eV, respectively. Reprinted from reference [56], an open access article under conditions of the Creative Commons Attribution (CC BY) license.

The energy distribution of Ti$_{ds}$ can also be obtained by an electrochemical method [61,62]. In this method, the potential variation in accumulated charge at the TiO$_2$ electrode can be measured in aqueous solution. By calculating the derivative of the accumulated charge (Q) versus the applied potential (U), the energy density of Ti$_{ds}$ is directly proportional to $\mathrm{d}Q/\mathrm{d}U$ and the plot of $\mathrm{d}Q/\mathrm{d}U$ vs. U reflects the energy distribution of Ti$_{ds}$. The maximum density of Ti$_{ds}$ is located around 0.25–0.4 eV below the CB edge for nanostructured anatase TiO$_2$ and P25 TiO$_2$ samples with a ratio of anatase to rutile of approximately 80:20. Thus, the distribution of Ti$_{ds}$ within 0–0.4 eV is predominant, so that electrons trapped in these trap states may participate in the reductive reaction on TiO$_2$.

4. Reactivity of Trapped and Accumulated Electrons

This section highlights the reactivity of electrons trapped at Ti$_{ds}$ and accumulated in CB in the reductions of molecular oxygen O$_2$ and molecular nitrogen N$_2$, and the hydrogenation and dehalogenation of selected organic substrates occurring on TiO$_2$. The reductive reactions associated with Ti$_{ds}$ have been extensively investigated under various experimental conditions and through theoretical calculation methods. Although many studies have been performed for clean surfaces on TiO$_2$ under high-vacuum conditions [17,18,30,57–59], here we focus on the reactions occurring on powder or colloidal TiO$_2$ under conventional gas or liquid phase conditions.

Here we define the terms 'accumulated electrons' (e_{cb}^-) and 'trapped electrons' ($\mathrm{Ti_{ds}}^{3+}$) to distinguish them. Accumulated electrons contain both electrons in CB and electrons trapped at shallow Ti states, located just below the CB edge of TiO$_{2,}$ within 0–0.05 eV. These electrons can be in thermal equilibrium between the bulk CB and at the shallow trap sites, and easily migrate through these states. The accumulation of electrons in these states should occur after saturation of the intra-bandgap Ti states (Ti$_{ds}$) during UV irradiation. These electrons are highly reactive at the TiO$_2$ interface (Step 4 in Figure 1).The trapped electrons $\mathrm{Ti_{ds}}^{3+}$ mean the electrons trapped at Ti$_{ds}$ are located in relatively deep energy from the CB edge. Therefore, the trapped electrons $\mathrm{Ti_{ds}}^{3+}$ cannot be excited thermally to the CB or the shallow states, exhibiting either low or no reactivity at the TiO$_2$ interface (Step 5 in Figure 1).

The trapped electrons $\mathrm{Ti_{ds}}^{3+}$ and the accumulated electrons e_{cb}^- are quite stable in the presence of a good sacrificial hole scavenger, such as alcohols or amines, and in the absence of electron acceptors such as O_2, the lifetime may exceed several hours [50,51,63]. This extremely long lifetime of $Ti_{ds}{}^{3+}$ and $e_{cb}{}^{-}$ is attributable to the excellent hole scavenging ability of the sacrificial reagents on the TiO_2 surface [24], which prevents the recombination of $Ti_{ds}{}^{3+}$ and $e_{cb}{}^{-}$ with the surface trapped holes. In other words, the hole scavengers inhibit Steps 7 and 8 in Figure 1. The excess charges caused by electrons $Ti_{ds}{}^{3+}$ and $e_{cb}{}^{-}$ on the irradiated TiO_2 are balanced by the insertion (intercalation) of protons into the TiO_2 lattice [47,62,64,65]. The electrons $Ti_{ds}{}^{3+}$ and $e_{cb}{}^{-}$ show the unique blue-black coloration from the visible to the IR region [14,40,42–51], which enables the tracing of the lifetimes of the species generated on the irradiated TiO_2. Interestingly, the electrons $Ti_{ds}{}^{3+}$ and $e_{cb}{}^{-}$ are distinguishable by measuring IR spectra. The free electrons $e_{cb}{}^{-}$ exhibit the typical exponential frequency-dependent spectrum that is attributed to the intra-CB transition [43,44,46,48], whereas the trapped electrons $Ti_{ds}{}^{3+}$ are characterized by a broad absorption in the mid-IR region that is ascribed to a direct optical transition [46,48].

4.1. Reduction of Molecular Oxygen and Hydrogen Peroxide

The interfacial electron transfer between molecular oxygen (O_2) and electrons $Ti_{ds}{}^{3+}$ or $e_{cb}{}^{-}$ on nanocrystalline TiO_2 films was examined using a transient UV–vis absorption spectroscopy in gas phase [66]. In the presence of ethanol, as a sacrificial hole scavenger under ethanol-saturated conditions (5.8%), the half-life ($t_{50\%}$) of the electron-species $Ti_{ds}{}^{3+}$ and $e_{cb}{}^{-}$ was approximately 0.5 s in the absence of O_2. The $t_{50\%}$ value drastically decreased with increasing O_2 concentration, to approximately 12 μs in an oxygen concentration of 21% (air saturated conditions). Thus, the efficient electron transfer of molecular oxygen in a gaseous phase occurred on TiO_2 films by using ethanol as the hole scavenger. The dynamics of the electron transfer between O_2 and the nanosized TiO_2 particles in a liquid phase were also investigated by employing a simple and facile stopped flow technique [50,51]. With methanol as the hole scavenger, the electrons on the TiO_2 particles, in an argon-purged and de-aerated aqueous solution, were accumulated by pre-UV irradiation, causing blue colorization characterized by a broad absorption band in the visible light region of 400–800 nm. In the stopped flow experiment, the TiO_2 solution containing the electron-species $Ti_{ds}{}^{3+}$ and $e_{cb}{}^{-}$ was mixed with the aqueous solution containing O_2 at pH2.3, and the change in absorbance of the electrons was recorded at 600 nm. The absorbance signal decreased slowly with a rate constant of 8.9×10^{-7} mol L^{-1} s^{-1} in the absence of O_2, whereas the signal rapidly disappeared within a few seconds under O_2-saturated conditions. Thus, efficient electron transfer from the accumulated TiO_2 to O_2 proceeded even in the aqueous solution. The reduction of hydrogen peroxide (H_2O_2) was also confirmed by the same stopped flow experiment [50,51]. The decay rate of the electron-species $Ti_{ds}{}^{3+}$ and $e_{cb}{}^{-}$ in the H_2O_2 reduction was slower than in the O_2 reduction under similar conditions.

The reduction of O_2 on TiO_2 results in the formation of reactive oxygen species (ROS), such as superoxide anion radicals ($O_2{}^{\cdot-}$), hydroperoxy radicals ($^{\cdot}OOH$), hydrogen peroxide (H_2O_2), and hydroxyl radicals ($^{\cdot}OH$), under both aqueous and aerated conditions [6,21]. These ROS play a crucial role in the photocatalysis on TiO_2 for water purification, air cleaning, self-cleaning, self-sterilization, etc. The sequential ROS generation on photo-irradiated TiO_2 under acidic conditions can be depicted as follows [6,21,50,51]:

Photoreduction:	$O_2 + (Ti_{ds}{}^{3+} \text{ and } e_{cb}{}^{-}) \rightarrow O_2{}^{\cdot-}$
Protonation:	$O_2{}^{\cdot-} + H^+ \rightarrow {}^{\cdot}OOH$
Disproportionation:	$2\,{}^{\cdot}OOH \rightarrow H_2O_2 + O_2$
Photoreduction:	$H_2O_2 + (Ti_{ds}{}^{3+} \text{ and } e_{cb}{}^{-}) \rightarrow {}^{\cdot}OH + OH^-$

Though the CB edge of anatase TiO_2 is located at −0.27 V vs. standard hydrogen electrode (SHE) at pH2.3 [67], anatase TiO_2 produced the superoxide anion radial by photoexcitation; $O_2/O_2{}^{\cdot-}$ was approximately 0.33 V vs. SHE [68]. This could be due to the strong adsorption of O_2 at the Ti_{ds} sites, such as $V_O^{\bullet\bullet}$, which may lead to a positive shift of the redox potential ($O_2/O_2{}^{\cdot-}$). In this electron transfer step, an electron seems to be transferred from the Ti 3d orbital to the π^* orbital of the adsorbed O_2.

4.2. Reduction of Molecular Nitrogen, Nitrate, and Nitrite Ions

Molecular nitrogen (N_2) is chemically stable, so photocatalytic reduction of N_2 to ammonia (NH_3) under ambient temperature and pressure is challenging. Hirakawa and coworkers recently reported that the photocatalytic conversion of N_2 to ammonia with water occurred on the bare TiO_2 powders under ambient conditions [69]. They stated that the active sites for N_2 reduction are the Ti_{ds} with oxygen vacancies mainly formed on the rutile {110} surface. They investigated the photocatalytic reductions of nitrate (NO_3^-) and nitrite (NO_2^-) ions to ammonia and N_2 on bare TiO_2 under ambient conditions [70]. They proposed that the Ti_{ds} sites selectively promoted the eight-electron reduction of NO_3^- to NH_3 ($NO_3^- + 9H^+ + 8e^- \rightarrow NH_3 + 3H_2O$), while the Lewis acid site promoted nonselective reduction, resulting in N_2 and NH_3 formation. Thus, TiO_2 with many Ti_{ds} and a small number of Lewis acid sites produced ammonia with very high selectivity. The use of artificial fertilizers in agriculture has caused a great deal of concern for water pollution caused by the production of NO_3^- and NO_2^- ions from fertilizers [71]. Therefore, a chemical process for the reduction of NO_3^- and NO_2^- ions on TiO_2 may be useful for an environmental recycling process.

4.3. Hydrogenation of Carbonyl Compounds

Kohtani et al. examined whether electrons Ti_{ds}^{3+} and e_{cb}^- transfer to acetophenone (AP) derivatives adsorbed on TiO_2 [63,72]. The photoreductive hydrogenation of several aromatic carbonyl compounds was confirmed to occur on UV-irradiated P25 TiO_2 as illustrated in Scheme 1 [72,73]. They evaluated the number of transferred electrons in the injection experiment using a pre-irradiated TiO_2 suspension. When the P25 TiO_2 powder was dispersed in de-aerated ethanol as a hole scavenger and irradiated with UV light for 2 h, the white color of TiO_2 powder changed to blue-gray. After the blue-gray color change was confirmed, a large amount of AP derivatives was injected into this TiO_2 suspension in the dark. In this experiment, ethanol acted not only as a solvent but also as a hole scavenger.

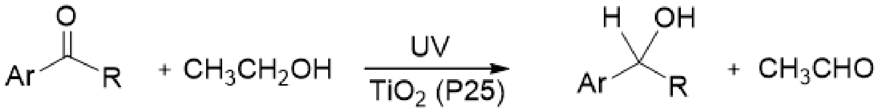

Scheme 1. Photocatalytic hydrogenation of aromatic carbonyl compounds: Ar = aromatic ring, R = H, Me, Et, *i*-Pr, or CF_3. Reprinted with permission from reference [72]. Copyright (2014) The Royal Society of Chemistry.

Figure 3a shows that the blue-gray color of the pre-irradiated P25 TiO_2 suspension remained for a few days in the absence of AP derivatives [63], meaning that the electrons accumulated on the P25 TiO_2 surface are quite stable in the de-aerated ethanol. Figure 3b,c show the color change induced by the addition of aromatic carbonyl compounds. The blue-gray color of TiO_2 rapidly changed after the injection of 2,2,2-trifluoacetophenone (TFAP) where the aromatic ring (Ar) was C_6H_5 and the R was CF_3 (Scheme 1). The change from blue-gray to white was completed within 3 h in the TFAP solution as shown in Figure 3c. This result indicates that all the trapped and accumulated electrons on TiO_2 were consumed in the reduction of TFAP within 3 h. On the other hand, with AP, a part of the blue-gray species on TiO_2 was remarkably stable even after 50 h, as shown in Figure 3b, which may be due to the remaining electrons trapped at the deep states of TiO_2.

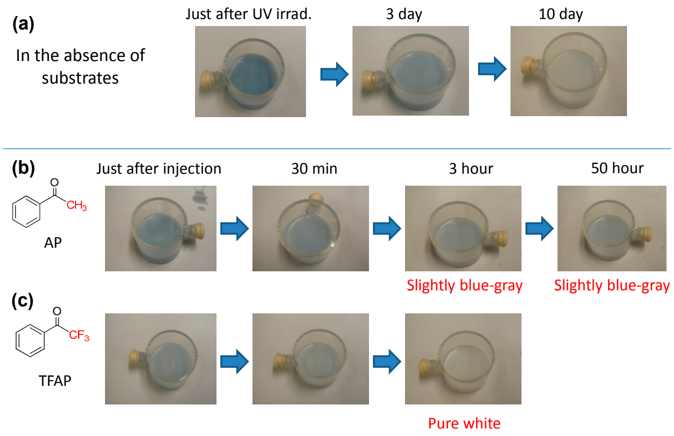

Figure 3. Color changes of the pre-irradiated P25 TiO_2 powder dispersed in de-aerated ethanol (**a**) in the absence of substrates, and after injection of (**b**) 300 μmol acetophenone (AP), or (**c**) 2,2,2-trifluoacetophenone (TFAP). Adapted with permission from reference [63]. Copyright 2012 American Chemical Society. UV irrad.: UV irraditaion.

Figure 4 depicts the time evolution of the secondary alcohols 1-phenylethanol (AP-OH) or 1-phenyl-2,2,2-trifluoroethanol (TFAP-OH), as products after the injection of substrates AP or TFAP, into the sufficient pre-irradiated TiO_2 suspension, respectively [63]. The amount of each product quickly grew within 0.5 h, which agrees with the observation of color change in the TiO_2 suspension (Figure 3b,c). The amount of TFAP-OH product obtained from the reactive substrate TFAP rapidly increased, and reached 5.4 μmoL within 1 h. Assuming all Ti_{ds}^{3+} and e_{cb}^{-} electrons were consumed in the reductive hydrogenation of TFAP, the total amount of Ti_{ds}^{3+} and e_{cb}^{-} on the TiO_2 powder was estimated to be about 100 $\mu mol \cdot g^{-1}$. The time evolution of AP-OH from the less reactive substrate AP consisted of a fast component within 0.5 h, and a slow component after 0.5 h, which increased gradually to reach 4.1 μmol (Figure 4). The slow component represents the slow electron transfer event from middle $Ti_{ds,}$ between shallow and deep states, to AP adsorbed on TiO_2. The total amount of AP-OH production was about 25% smaller than that of TFAP-OH production. In the reduction of the less reactive substrate AP, the deep Ti_{ds}^{3+} species remained on the TiO_2 surface for a long time (>20 h) after the injection of AP. The amount of deep Ti_{ds}^{3+} that remained on TiO_2 was roughly estimated to be 25% given the difference between the amounts of TFAP-OH (5.4 μmoL) and AP-OH (4.1 μmoL). Thus, the residual 25% electrons could not react with AP and remained at the deep trap sites.

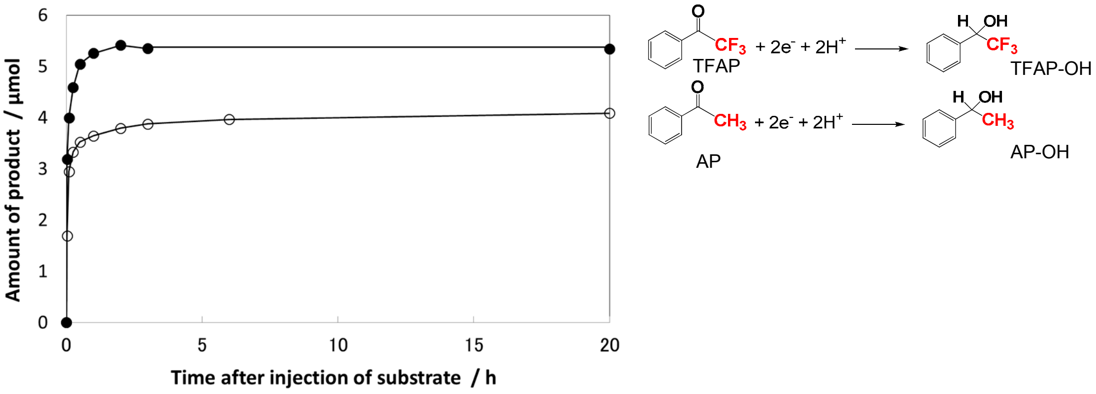

Figure 4. Time evolutions of the amount of AP-OH (○) and TFAP-OH (●) after the 300 μmol injection of substrate (AP or TFAP) into the 2 h pre-irradiated TiO_2 suspension at 32 °C Adapted with permission from reference [63]. Copyright (2012) American Chemical Society.

Assuming that all Ti_{ds}^{3+} and e_{cb}^{-} electrons react with TFAP, the percentages of reacted electrons were estimated for other AP derivatives, as summarized in Table 1 [72]. The number of reacted electrons showed a tendency to decrease with decreasing the reduction potential (E_{red}) of the substrates according to the dependence on the actual reaction rates as listed in Table 1. This implies that the rates of photocatalytic hydrogenation of AP derivatives are governed by the electron transfer efficiency from the Ti_{ds} sites to the adsorbed AP sites. Notably, the relative position between the Ti_{ds} energy distributed within the bandgap and the acceptor level of the AP derivatives (the solid Gaussian curve) should be appropriate (Figure 5) [72]. The energy distribution of Ti_{ds} in TiO_2 powders and colloids can be obtained by photochemical [60], electrochemical [61,62], and RDB-PAS [56] methods. The acceptor levels of AP derivatives can be estimated by the Marcus theory [72,74–76].

Table 1. Reduction potentials, amount of reacted electrons, percentages of reacted electrons, and reaction rates at maximum concentration of substrates [72]. Adapted with permission from reference [72]. Copyright (2014) The Royal Society of Chemistry.

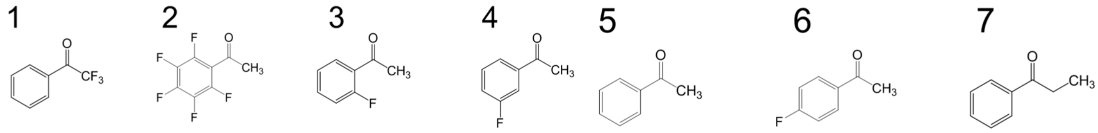

Substrate	E_{red}/V [a]	Amount of Reacted Electrons [b]/μmoL	Percentage [c]/%	Reaction Rate [d]/mMh^{-1}
1 (TFAP)	–1.35	10.2	100	–
2	–1.59	8.22	81	3.4 ± 0.2
3	–1.62	6.32	62	2.2 ± 0.2
4	–1.80	6.09	60	2.0 ± 0.1
5 (AP)	–1.89	7.38	72	1.9 ± 0.1
6	–0.92	5.70	56	1.2 ± 0.1
7	–1.94	4.76	47	0.75 ± 0.05

[a] Reduction potentials vs. SHE (standard hydrogen electrode). [b] Molar number of reacted electrons estimated by the injection experiment using a pre-irradiated TiO_2 suspension. [c] Percentage of the reacted electrons per the total amount of Ti_{st}^{3+} and e_{cb}^{-} (10.2 μmol) generated on 0.10 g TiO_2. [d] Reaction rates at the maximum concentration of substrates.

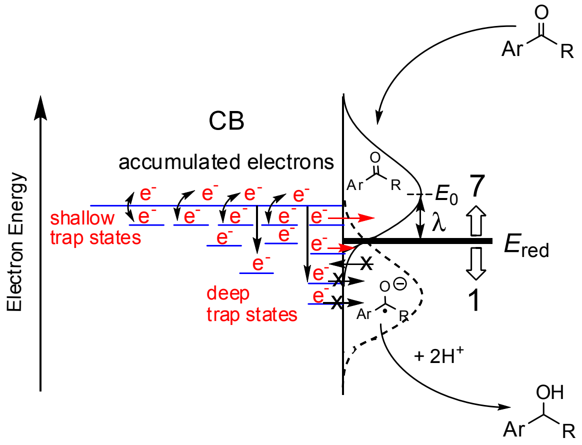

Figure 5. Schematic illustration of the electron transfer reaction from the Ti_{ds} states to the adsorbed AP derivatives, where E_{red} is the reduction potential of AP derivatives, λ is the reorganization energy (approximately 0.7 eV for AP), and E_0 is the energy at the top of curve for the acceptor level, calculated by $qE_{red} - \lambda$ and shown by the solid line. The dotted line indicates the donor energy level for anionic species. Reprinted with permission from reference [72]. Copyright (2014) The Royal Society of Chemistry.

Kohtani et al. also reported the photohydrogenation of AP derivatives on P25 $TiO_{2,}$ modified with metal-free organic dyes such as rhodamine B, fluorescein, and coumarin derivatives [77,78]. The use of these organic dyes successfully extended the UV response of TiO_2 to the visible light region, though these reaction rates were much slower than the hydrogenation rate using UV excitation of non-modified TiO_2. In this dye-sensitized system, the electron injection from dye into TiO_2 can take place in two different ways: (1) injection via a lowest unoccupied molecular orbital (LUMO) level of the excited dye to the CB of TiO_2, and (2) direct injection of TiO_2 to CB on the excitation of the charge transfer complex ($TiO_2^{\delta-}$ dye$^{\delta+}$) [77]. The injected electrons should then be distributed to the Ti_{ds} sites on the P25 TiO_2 surface. The accumulated electrons were observed with the blue-gray color for all dye-TiO_2 powders during visible light irradiation.

4.4. Defluorination of Fluorinated AP Derivatives

Compounds containing fluorine atoms are often used as pharmaceutical and agrochemical reagents. Since the C–F bond is one of the strongest bonds, C–F bond activation and cleavage is a field of current interest in organic chemistry [79], although less is known about the catalytic activation and cleavage methods. Photocatalytic reaction is one of the promising methods to promote the activation and cleavage of the C–F bond of fluorinated compounds under mild conditions. Therefore, an attempt was made to use trapped and accumulated electrons on TiO_2 for the sequential multi-step electron transfer in the reduction of fluorinated AP derivatives (Figure 6) [80]. The reaction of fluorinated AP derivatives on TiO_2 showed the two photocatalytic reductive transformations, i.e., the defluorination and reduction of the carbonyl group. The reduction of 2-fluoromethylacetophenone (MFAP) only provided the ketone AP because of the C–F bond cleavage, whereas the reaction of TFAP only provided the alcohol TFAP-OH as a result of the reduction of the carbonyl group. Interestingly, the reduction of 2,2-difluoromethyacetophenone (DFAP), possessing characteristics between those of MFAP and TFAP, gave the defluorinated ketones, MFAP and AP, as well as hydrogenated alcohol 1-phenyl-2,2-difluoroethanol (DFAP-OH), as shown in Figure 6. The defluorination reactions became unfavorable with increasing the number of fluorine atoms on the substrates. This mainly arises because of the increase in the bond dissociation energy of the C–F bond and the positive shift of the reduction potential of fluorinated AP derivatives with the increasing number of fluorine atoms [80].

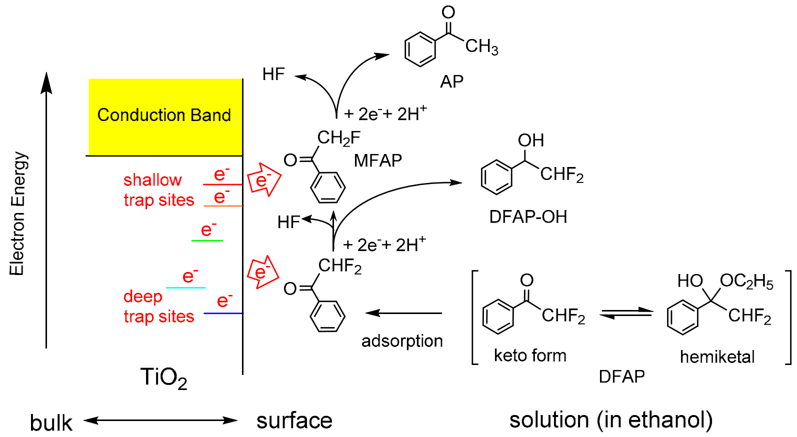

Figure 6. Schematic illustration on the photocatalytic reduction of 2,2-difluoromethyacetophenone (DFAP) on the UV irradiated TiO_2. Reprinted with permission from reference [80]. Copyright (2016) Elsevier B.V.

4.5. Hydrogenation of Nitroaromatic Compounds

Several organic nitroaromatic compounds can be easily hydrogenated to create the corresponding amino compounds on the UV-irradiated TiO_2 in the presence of 2-propanol as a sacrificial hole scavenger (Scheme 2).

Reduction

$$Ar{-}NO_2 + 6e^- + 6H^+ \longrightarrow Ar{-}NH_2 + 2H_2O$$

Oxidation

$$3(CH_3)_2CHOH + 6h^+ \longrightarrow 3(CH_3)_2CO + 6H^+$$

Scheme 2. Photocatalytic reduction of nitroaromatic compounds and oxidation of 2-propanol as a sacrificial hole scavenger.

Shiraishi et al. reported that some kinds of rutile TiO_2 particles promote the highly efficient photocatalytic hydrogenation of nitroaromatic compounds [81,82]. They claimed that the oxygen vacancy sites on the rutile {110} behave as the adsorption sites for the nitroaromatic compounds and the electron trap sites, resulting in the formation of aniline derivatives with significantly high yields of greater than 25% at 370 nm [81]. They also found that the activity of rutile particles depends on the number of defects on the particles [82]. The inner (bulk) defects behave as the deactivation sites for the recombination of electrons and holes, whereas the surface defects behave as the active reaction sites as well as the deactivation sites. As a result, the reaction rate is proportional to the ratio of the amount of surface defects to that of total defects ($N_{surface}/N_{total}$) in the rutile TiO_2 particles, which aligns with the report of Kong and coworkers [16].

Molinari and coworkers examined the selective hydrogenation of NO_2–C_6H_4–CHO, bearing the two reducible functional groups, –NO_2 and –CHO [62]. They found that the nitro group was easily reduced by the trapped electrons at Ti_{ds} within the bandgap, whereas the aldehyde group was reduced by electrons accumulated on CB. Therefore, the chemoselective reduction of functional groups can be controlled by the energy distribution patterns of Ti_{ds}, which may depend on the type of TiO_2 powders. The selective reduction of functional groups is difficult to achieve through conventional thermal catalysis. Therefore, this topic is an interesting issue for chemoselective photocatalysis.

5. Summary and Potential for the Development of Efficient Photocatalysis

According to the reports of Kong et al. [16] and Shiraishi et al. [82], the photocatalytic efficiencies increased with increasing the ratio of the amount of surface to bulk defects ($N_{surface}/N_{bulk}$) or the amount of surface to total defects ($N_{surface}/N_{total}$). For example, molecular oxygen (O_2) in a gaseous phase would be easily adsorbed on the surface Ti_{ds} and reduced by electrons ${Ti_{ds}}^{3+}$ and ${e_{cb}}^-$, resulting in the efficient formation of ROS, which oxidize benzene efficiently [16]. Further, the surface Ti_{ds} behaves as the active reaction site in the efficient reduction of nitrobenzene [81]. Thus, the surface defects favorably act as adsorption sites as well as reaction sites.

In addition, the relative position between the energy distributions of Ti_{ds} and the acceptor level (reduction potential) of substrates should be appropriate as indicated in Figure 5 [72]. The electrons accumulated in CB and trapped at shallow Ti_{ds} can easily participate in the reaction, whereas those trapped at deep Ti_{ds} cannot [63]. These unreacted electrons remain at the deep Ti_{ds} sites and exhibit an extremely long lifetime in alcohols. Thus, the shallow traps enhance photocatalytic activity, while the deep traps cause a reduction. Furthermore, Amano et al. proposed that the creation of shallow Ti_{ds} greatly enhances electrical conductivity, thereby facilitating the charge transport and separation caused by the formation of band bending in the space charge layer at the TiO_2-liquid interface [14,15].

In conclusion, the development of highly active photocatalysts necessitates precise control of the structural properties; the density of surface shallow traps should be maximized and the density of deep traps as well as inner (bulk) traps minimized, as proposed by Ohtani [83]. One of the promising strategies for meeting these requirements is the use of highly uniform TiO_2 nanocrystals with specific exposure of the reactive facets [42,84–87]. In particular, the anatase {101} and {001} facets have been reported to be favorable for the reductive and oxidative reactions in TiO_2 photocatalysis, respectively [87–91]. If the reductive and oxidative facets could be selectively covered with a large amount of the active shallow Ti_{ds} and the terminal $Ti–O_sH$ hole trapping sites, respectively, the photocatalytic activity on the TiO_2 nanocrystals would be greatly enhanced by the effective electron-hole charge separation, followed by the subsequent charge transfer reactions at the specific reductive and oxidative sites. Therefore, special attention should be directed toward the development of TiO_2 nanocrystals with precisely controlled facets.

Acknowledgments: The works in references [63,72,73,77,78,80] were supported by JSPS KAKENHI Grant Numbers 21590052 and 24590067.

Conflicts of Interest: The author declares no conflict of interest.

References

1. Fujishima, A.; Honda, K. Electrochemical photolysis of water at a semiconductor electrode. *Nature* **1972**, *238*, 37–38. [CrossRef] [PubMed]
2. Kudo, A.; Miseki, Y. Heterogeneous photocatalyst materials for water splitting. *Chem. Soc. Rev.* **2009**, *38*, 253–278. [CrossRef] [PubMed]
3. Fujishima, A.; Zhang, X.; Tryk, D. Heterogeneous photocatalysis: From water photolysis to applications in environmental cleanup. *Int. J. Hydrog. Energy* **2007**, *32*, 2664–2672. [CrossRef]
4. Grätzel, M. Recent advances in sensitized mesoscopic solar cells. *Acc. Chem. Res.* **2009**, *42*, 1788–1798. [CrossRef] [PubMed]
5. Hagfeldt, A.; Boschloo, G.; Sun, L.; Kloo, L.; Pettersson, H. Dye-sensitized solar cells. *Chem. Rev.* **2010**, *110*, 6595–6663. [CrossRef] [PubMed]
6. Hoffmann, M.; Martin, S.; Choi, W.; Bahnemann, D. Environmental applications of semiconductor photocatalysis. *Chem. Rev.* **1995**, *95*, 69–96. [CrossRef]
7. Sakata, T. Photocatalysis of irradiated semiconductor surfaces: Its application to water splitting and some organic reactions. *J. Photochem.* **1985**, *29*, 205–215. [CrossRef]
8. Kisch, H. Semiconductor photocatalysis for organic synthesis advances in photochemistry. *Adv. Photochem.* **2001**, *26*, 93–143.
9. Palmisano, G.; Augugliaro, V.; Pagliaro, M.; Palmisano, L. Photocatalysis: A promising route for 21st century organic chemistry. *Chem. Commun.* **2007**, 3425–3437. [CrossRef] [PubMed]
10. Kohtani, S.; Yoshioka, E.; Miyabe, H. Photocatalytic hydrogenation on semiconductor particles. *Hydrogenation* **2012**, 291–308. [CrossRef]
11. Kisch, H. Semiconductor photocatalysis-mechanistic and synthetic aspects. *Angew. Chem. Int. Ed.* **2013**, *52*, 812–847. [CrossRef] [PubMed]
12. Fujishima, A.; Rao, T.; Tryk, D. Titanium dioxide photocatalysis. *J. Photochem. Photobiol. C* **2000**, *1*, 1–21. [CrossRef]
13. Thompson, T.; Yates, J. Surface science studies of the photoactivation of TiO_2 new photochemical processes. *Chem. Rev.* **2006**, *106*, 4428–4453. [CrossRef] [PubMed]
14. Amano, F.; Nakata, M.; Yamamoto, A.; Tanaka, T. Effect of Ti^{3+} ions and conduction band electrons on photocatalytic and photoelectrochemical activity of rutile titania for water oxidation. *J. Phys. Chem. C* **2016**, *120*, 6467–6474. [CrossRef]
15. Amano, F.; Nakata, M.; Yamamoto, A.; Tanaka, T. Rutile titanium dioxide prepared by hydrogen reduction of degussa P25 for highly efficient photocatalytic hydrogen evolution. *Catal. Sci. Technol.* **2016**, *6*, 5693–5699. [CrossRef]
16. Kong, M.; Li, Y.; Chen, X.; Tian, T.; Fang, P.; Zheng, F.; Zhao, X. Tuning the relative concentration ratio of bulk defects to surface defects in TiO_2 nanocrystals leads to high photocatalytic efficiency. *J. Am. Chem. Soc.* **2011**, *133*, 16414–16417. [CrossRef] [PubMed]
17. Diebold, U. The surface science of titanium dioxide. *Surf. Sci. Rep.* **2003**, *48*, 53–229. [CrossRef]

18. Henderson, M. A Surface science perspective on TiO_2 photocatalysis. *Surf. Sci. Rep.* **2011**, *66*, 185–297. [CrossRef]
19. Nowotny, M.K.; Sheppard, L.R.; Bak, T.; Nowotny, J. Defect chemistry of titanium dioxide. Application of defect engineering in processing of TiO_2-based photocatalysts. *J. Phys. Chem. C* **2008**, *112*, 5275–5300. [CrossRef]
20. Nowotny, J.; Alim, M.; Bak, T.; Idris, M.; Ionescu, M.; Prince, K.; Sahdan, M.; Sopian, K.; Mat Teridi, M.; Sigmund, W. Defect chemistry and defect engineering of TiO_2-based semiconductors for solar energy conversion. *Chem. Soc. Rev.* **2015**, *44*, 8424–8442. [CrossRef] [PubMed]
21. Schneider, J.; Matsuoka, M.; Takeuchi, M.; Zhang, J.; Horiuchi, Y.; Anpo, M.; Bahnemann, D. Understanding TiO_2 photocatalysis: Mechanisms and materials. *Chem. Rev.* **2014**, *114*, 9919–9986. [CrossRef] [PubMed]
22. Tamaki, Y.; Furube, A.; Murai, M.; Hara, K.; Katoh, R.; Tachiya, M. Dynamics of efficient electron-hole separation in TiO_2 nanoparticles revealed by femtosecond transient absorption spectroscopy under the weak-excitation condition. *Phys. Chem. Chem. Phys.* **2007**, *9*, 1453–1460. [CrossRef] [PubMed]
23. Tamaki, Y.; Hara, K.; Katoh, R.; Tachiya, M.; Furube, A. Femtosecond visible-to-IR spectroscopy of TiO_2 nanocrystalline films: Elucidation of the electron mobility before deep trapping. *J. Phys. Chem. C* **2009**, *113*, 11741–11746. [CrossRef]
24. Tamaki, Y.; Furube, A.; Murai, M.; Hara, K.; Katoh, R.; Tachiya, M. Direct observation of reactive trapped holes in TiO_2 undergoing photocatalytic oxidation of adsorbed alcohols: Evaluation of the reaction rates and yields. *J. Am. Chem. Soc.* **2006**, *128*, 416–417. [CrossRef] [PubMed]
25. Ma, Y.; Wang, X.; Jia, Y.; Chen, X.; Han, H.; Li, C. Titanium dioxide-based nanomaterials for photocatalytic fuel generations. *Chem. Rev.* **2014**, *114*, 9987–10043. [CrossRef] [PubMed]
26. Chen, X.; Liu, L.; Yu, P.Y.; Mao, S.S. Increasing solar absorption for photocatalysis with black hydrogenated titanium dioxide nanocrystals. *Science* **2011**, *331*, 746–750. [CrossRef] [PubMed]
27. Chen, X.; Liu, L.; Huang, F. Black titanium dioxide (TiO_2) nanomaterials. *Chem. Soc. Rev.* **2015**, *44*, 1861–1885. [CrossRef] [PubMed]
28. Zhou, W.; Li, W.; Wang, J.-Q.; Qu, Y.; Yang, Y.; Xie, Y.; Zhang, K.; Wang, L.; Fu, H.; Zhao, D. Ordered mesoporous black TiO_2 as highly efficient hydrogen evolution photocatalyst. *J. Am. Chem. Soc.* **2014**, *136*, 9280–9283. [CrossRef] [PubMed]
29. Di Valentin, C.; Pacchioni, G.; Selloni, A. Reduced and n-type doped TiO_2: Nature of Ti^{3+} species. *J. Phys. Chem. C* **2009**, *113*, 20543–20552. [CrossRef]
30. Wendt, S.; Sprunger, P.T.; Lira, E.; Madsen, G.K.H.; Li, Z.; Hansen, J.O.; Matthiesen, J.; Blekinge Rasmussen, A.; Laegsgaard, E.; Hammer, B.; et al. The role of interstitial sites in the Ti*3d* defect state in the band gap of titania. *Science* **2008**, *320*, 1755–1759. [CrossRef] [PubMed]
31. Chen, X.; Zhao, D.; Liu, K.; Wang, C.; Liu, L.; Li, B.; Zhang, Z.; Shen, D. Laser-modified black titanium oxide nanospheres and their photocatalytic activities under visible light. *ACS Appl. Mater. Interfaces* **2015**, *7*, 16070–16077. [CrossRef] [PubMed]
32. Filice, S.; Compagnini, G.; Fiorenza, R.; Scirè, S.; D'Urso, L.; Fragalà, M.E.; Russo, P.; Fazio, E.; Scalese, S. Laser processing of TiO_2 colloids for an enhanced photocatalytic water splitting activity. *J. Colloid Interface Sci.* **2017**, *489*, 131–137. [CrossRef] [PubMed]
33. Russo, P.; Liang, R.; He, R.X.; Zhou, Y.N. Phase transformation of TiO_2 nanoparticles by femtosecond laser ablation in aqueous solutions and deposition on conductive substrates. *Nanoscale* **2017**, *9*, 6167–6177. [CrossRef] [PubMed]
34. Zhang, D.; Liu, J.; Li, P.; Tian, Z.; Liang, C. Recent advances in surfactant-free, surface-charged, and defect-rich catalysts developed by laser ablation and processing in liquids. *ChemNanoMat* **2017**, *3*, 512–533. [CrossRef]
35. Weiler, B.; Gagliardi, A.; Lugli, P. Kinetic monte carlo simulations of defects in anatase titanium dioxide. *J. Phys. Chem. C* **2016**, *120*, 10062–10077. [CrossRef]
36. Deskins, N.A.; Rousseau, R.; Dupuis, M. Localized electronic states from surface hydroxyls and polarons in TiO_2 (110). *J. Phys. Chem. C* **2009**, *113*, 14583–14586. [CrossRef]
37. Deskins, N.A.; Rousseau, R.; Dupuis, M. Distribution of Ti^{3+} surface sites in reduced TiO_2. *J. Phys. Chem. C* **2011**, *115*, 7562–7572. [CrossRef]
38. Howe, R.; Grätzel, M. EPR observation of trapped electrons in colloidal titanium dioxide. *J. Phys. Chem.* **1985**, *89*, 4495–4499. [CrossRef]

39. Hurum, D.; Agrios, A.; Gray, K.; Rajh, T.; Thurnauer, M. Explaining the enhanced photocatalytic activity of degussa P25 mixed-phase TiO_2 using EPR. *J. Phys. Chem. B* **2003**, *107*, 4545–4549. [CrossRef]
40. Berger, T.; Sterrer, M.; Diwald, O.; Knözinger, E.; Panayotov, D.; Thompson, T.L.; Yates, J.T. Light-induced charge separation in anatase TiO_2 particles. *J. Phys. Chem. B* **2005**, *109*, 6061–6068. [CrossRef] [PubMed]
41. Li, G.; Dimitrijevic, N.; Chen, L.; Nichols, J.; Rajh, T.; Gray, K. The important role of tetrahedral Ti^{4+} sites in the phase transformation and photocatalytic activity of TiO_2 nanocomposites. *J. Am. Chem. Soc.* **2008**, *130*, 5402–5403. [CrossRef] [PubMed]
42. Gordon, T.; Cargnello, M.; Paik, T.; Mangolini, F.; Weber, R.; Fornasiero, P.; Murray, C. Nonaqueous synthesis of TiO_2 nanocrystals using TiF_4 to engineer morphology, oxygen vacancy concentration, and photocatalytic activity. *J. Am. Chem. Soc.* **2012**, *134*, 6751–6761. [CrossRef] [PubMed]
43. Szczepankiewicz, S.; Colussi, A.J.; Hoffmann, M. Infrared spectra of photoinduced species on hydroxylated titania surfaces. *J. Phys. Chem. B* **2000**, *104*, 9842–9850. [CrossRef]
44. Szczepankiewicz, S.; Moss, J.; Hoffmann, M. Slow surface charge trapping kinetics on irradiated TiO_2. *J. Phys. Chem. B* **2002**, *106*, 2922–2927. [CrossRef]
45. Takeuchi, M.; Martra, G.; Coluccia, S.; Anpo, M. Verification of the photoadsorption of H_2O molecules on TiO_2 semiconductor surfaces by vibrational absorption spectroscopy. *J. Phys. Chem. C* **2007**, *111*, 9811–9817. [CrossRef]
46. Panayotov, D.; Burrows, S.; Morris, J. Infrared spectroscopic studies of conduction band and trapped electrons in UV-photoexcited, H-atom n-doped, and thermally reduced TiO_2. *J. Phys. Chem. C* **2012**, *116*, 4535–4544. [CrossRef]
47. Savory, D.; McQuillan, A.J. Influence of formate adsorption and protons on shallow trap infrared absorption (STIRA) of anatase TiO_2 during photocatalysis. *J. Phys. Chem. C* **2013**, *117*, 23645–23656. [CrossRef]
48. Litke, A.; Hensen, E.J.M.; Hofmann, J. Role of dissociatively adsorbed water on the formation of shallow trapped electrons in TiO_2 photocatalysts. *J. Phys. Chem. C* **2017**, *121*, 10153–10162. [CrossRef] [PubMed]
49. Takeuchi, M.; Deguchi, J.; Sakai, S.; Anpo, M. Effect of H_2O vapor addition on the photocatalytic oxidation of ethanol, acetaldehyde and acetic acid in the gas phase on TiO_2 semiconductor powders. *Appl. Catal. B Environ.* **2010**, *96*, 218–223. [CrossRef]
50. Mohamed, H.; Dillert, R.; Bahnemann, D. Reaction dynamics of the transfer of stored electrons on TiO_2 nanoparticles: A stopped flow study. *J. Photochem. Photobiol. A Chem.* **2011**, *217*, 271–274. [CrossRef]
51. Mohamed, H.; Mendive, C.; Dillert, R.; Bahnemann, D. Kinetic and mechanistic investigations of multielectron transfer reactions induced by stored electrons in TiO_2 nanoparticles: A stopped flow study. *J. Phys. Chem. A* **2011**, *115*, 2139–2147. [CrossRef] [PubMed]
52. Knorr, F.; Mercado, C.; McHale, J. Trap-state distributions and carrier transport in pure and mixed-phase TiO_2: Influence of contacting solvent and interphasial electron transfer. *J. Phys. Chem. C* **2008**, *112*, 12786–12794. [CrossRef]
53. Leytner, S.; Hupp, J. Evaluation of the energetics of electron trap states at the nanocrystalline titanium dioxide/aqueous solution interface via time-resolved photoacoustic spectroscopy. *Chem. Phys. Lett.* **2000**, *330*, 231–236. [CrossRef]
54. Murakami, N.; Prieto Mahaney, O.; Torimoto, T.; Ohtani, B. Photoacoustic spectroscopic analysis of photoinduced change in absorption of titanium(IV) oxide photocatalyst powders: A novel feasible technique for measurement of defect density. *Chem. Phys. Lett.* **2006**, *426*, 204–208. [CrossRef]
55. Murakami, N.; Prieto Mahaney, O.; Abe, R.; Torimoto, T.; Ohtani, B. Double-beam photoacoustic spectroscopic studies on transient absorption of titanium(IV) oxide photocatalyst powders. *J. Phys. Chem. C* **2007**, *111*, 11927–11935. [CrossRef]
56. Nitta, A.; Takase, M.; Takashima, M.; Murakami, N.; Ohtani, B. A fingerprint of metal-oxide powders: Energy-resolved distribution of electron traps. *Chem. Commun.* **2016**, *52*, 12096–12099. [CrossRef] [PubMed]
57. Pang, C.; Lun Pang, C.; Lindsay, R.; Thornton, G. Chemical reactions on rutile TiO_2 (110). *Chem. Soc. Rev.* **2008**, *37*, 2328–2353. [CrossRef] [PubMed]
58. Papageorigiou, A.; Papageorgiou, A.C.; Beglitis, N.S.; Pang, C.L.; Teobaldi, G.; Cabailh, G.; Chen, Q.; Fisher, A.J.; Hofer, W.A.; Thornton, G. Electron traps and their effect on the surface chemistry of TiO_2 (110). *Proc. Natl. Acad. Sci. USA* **2010**, *107*, 2391–2396. [CrossRef] [PubMed]
59. Setvin, M.; Aschauer, U.; Scheiber, P.; Li, Y.F.; Hou, W.; Schmid, M.; Selloni, A.; Diebold, U. Reaction of O_2 with subsurface oxygen vacancies on TiO_2 anatase (101). *Science* **2013**, *341*, 988–991. [CrossRef] [PubMed]

60. Ikeda, S.; Sugiyama, N.; Murakami, S.; Kominami, H.; Kera, Y.; Noguchi, H.; Uosaki, K.; Torimoto, T.; Ohtani, B. Quantitative analysis of defective sites in titanium(IV) oxide photocatalyst powders. *Phys. Chem. Chem. Phys.* **2003**, *5*, 778–783. [CrossRef]
61. Wang, H.; He, J.; Boschloo, G.; Lindström, H.; Hagfeldt, A.; Lindquist, S.-E. Electrochemical investigation of traps in a nanostructured TiO_2 film. *J. Phys. Chem. B* **2001**, *105*, 2529–2533. [CrossRef]
62. Molinari, A.; Maldotti, A.; Amadelli, R. Probing the role of surface energetics of electrons and their accumulation in photoreduction processes on TiO_2. *Chem. Eur. J.* **2014**, *20*, 7759–7765. [CrossRef] [PubMed]
63. Kohtani, S.; Yoshioka, E.; Saito, K.; Kudo, A.; Miyabe, H. Adsorptive and kinetic properties on photocatalytic hydrogenation of aromatic ketones upon UV irradiated polycrystalline titanium dioxide: Differences between acetophenone and its trifluoromethylated derivative. *J. Phys. Chem. C* **2012**, *116*, 17705–17713. [CrossRef]
64. Lemon, B.; Hupp, J. Photochemical quartz crystal microbalance study of the nanocrystalline titanium dioxide semiconductor electrode/water interface: Simultaneous photoaccumulation of electrons and protons. *J. Phys. Chem.* **1996**, *100*, 14578–14580. [CrossRef]
65. Jimenez, J.; Jiménez, J.; Bourret, G.; Berger, T.; McKenna, K. Modification of charge trapping at particle/particle interfaces by electrochemical hydrogen doping of nanocrystalline TiO_2. *J. Am. Chem. Soc.* **2016**, *138*, 15956–15964. [CrossRef] [PubMed]
66. Peiró, A.; Colombo, C.; Doyle, G.; Nelson, J.; Mills, A.; Durrant, J. Photochemical reduction of oxygen adsorbed to nanocrystalline TiO_2 films: A transient absorption and oxygen scavenging study of different TiO_2 preparations. *J. Phys. Chem. B* **2006**, *110*, 23255–23263. [CrossRef] [PubMed]
67. Dung, D.; Ramsden, J.; Grätzel, M. Dynamics of interfacial electron-transfer processes in colloidal semiconductor systems. *J. Am. Chem. Soc.* **1982**, *104*, 2977–2985. [CrossRef]
68. Ilan, Y.; Meisel, D.; Czapski, G. The redox potential of the O_2/O_2^- system in aqueous media. *Isr. J. Chem.* **1974**, *12*, 891–895. [CrossRef]
69. Hirakawa, H.; Hashimoto, M.; Shiraishi, Y.; Hirai, T. Photocatalytic conversion of nitrogen to ammonia with water on surface oxygen vacancies of titanium dioxide. *J. Am. Chem. Soc.* **2017**, *139*, 10929–10936. [CrossRef] [PubMed]
70. Hirakawa, H.; Hashimoto, M.; Shiraishi, Y.; Hirai, T. Selective nitrate-to-ammonia transformation on surface defects of titanium dioxide photocatalysts. *ACS Catal.* **2017**, *7*, 3713–3720. [CrossRef]
71. Burt, T.P.; Howden, N.J.K.; Worrall, F.; Whelan, M.J. Long-term monitoring of river water nitrate: How much data do we need? *J. Environ. Monit.* **2010**, *12*, 71–79. [CrossRef] [PubMed]
72. Kohtani, S.; Kamoi, Y.; Yoshioka, E.; Miyabe, H. Kinetic study on photocatalytic hydrogenation of acetophenone derivatives on titanium dioxide. *Catal. Sci. Technol.* **2014**, *4*, 1084–1091. [CrossRef]
73. Kohtani, S.; Yoshioka, E.; Saito, K.; Kudo, A.; Miyabe, H. Photocatalytic hydrogenation of acetophenone derivatives and diaryl ketones on polycrystalline titanium dioxide. *Catal. Commun.* **2010**, *11*, 1049–1053. [CrossRef]
74. Lewis, N. Progress in understanding electron-transfer reactions at semiconductor/liquid interfaces. *J. Phys. Chem. B* **1998**, *102*, 4843–4855. [CrossRef]
75. Hamann, T.; Gstrein, F.; Brunschwig, B.; Lewis, N. Measurement of the free-energy dependence of interfacial charge-transfer rate constants using ZnO/H_2O semiconductor/liquid contacts. *J. Am. Chem. Soc.* **2005**, *127*, 7815–7824. [CrossRef] [PubMed]
76. Ondersma, J.; Hamann, T. Measurements and modeling of recombination from nanoparticle TiO_2 electrodes. *J. Am. Chem. Soc.* **2011**, *133*, 8264–8271. [CrossRef] [PubMed]
77. Kohtani, S.; Nishioka, S.; Yoshioka, E.; Miyabe, H. Dye-sensitized photo-hydrogenation of aromatic ketones on titanium dioxide under visible light irradiation. *Catal. Commun.* **2014**, *43*, 61–65. [CrossRef]
78. Kohtani, S.; Mori, M.; Yoshioka, E.; Miyabe, H. Photohydrogenation of acetophenone using coumarin dye-sensitized titanium dioxide under visible light irradiation. *Catalysts* **2015**, *5*, 1417–1424. [CrossRef]
79. Beier, P.; Alexandrova, A.; Zibinsky, M.; Surya Prakash, G.K. Nucleophilic difluoromethylation and difluoromethylenation of aldehydes and ketones using diethyl difluoromethylphosphonate. *Tetrahedron* **2008**, *64*, 10977–10985. [CrossRef] [PubMed]
80. Kohtani, S.; Kurokawa, T.; Yoshioka, E.; Miyabe, H. Photoreductive transformation of fluorinated acetophenone derivatives on titanium dioxide: Defluorination vs. reduction of carbonyl group. *Appl. Catal. A Genel.* **2016**, *521*, 68–74. [CrossRef]

81. Shiraishi, Y.; Togawa, Y.; Tsukamoto, D.; Tanaka, S.; Hirai, T. Highly efficient and selective hydrogenation of nitroaromatics on photoactivated rutile titanium dioxide. *ACS Catal.* **2012**, *2*, 2475–2481. [CrossRef]
82. Shiraishi, Y.; Hirakawa, H.; Togawa, Y.; Sugano, Y.; Ichikawa, S.; Hirai, T. Rutile crystallites isolated from Degussa (Evonik) P25 TiO_2: Highly efficient photocatalyst for chemoselective hydrogenation of nitroaromatics. *ACS Catal.* **2013**, *3*, 2318–2326. [CrossRef]
83. Ohtani, B. Titania photocatalysis beyond recombination: A critical review. *Catalysts* **2013**, *3*, 942–953. [CrossRef]
84. Yang, H.; Sun, C.; Qiao, S.; Zou, J.; Liu, G.; Smith, S.; Cheng, H.; Lu, G. Anatase TiO_2 single crystals with a large percentage of reactive facets. *Nature* **2008**, *453*, 638–641. [CrossRef] [PubMed]
85. Amano, F.; Yasumoto, T.; Prieto Mahaney, O.-O.; Uchida, S.; Shibayama, T.; Ohtani, B. Photocatalytic activity of octahedral single-crystalline mesoparticles of anatase titanium(IV) oxide. *Chem. Commun.* **2009**, 2311–2313. [CrossRef] [PubMed]
86. Liu, G.; Yang, H.; Pan, J.; Yang, Y.; Lu, G.Q.; Cheng, H.-M. Titanium dioxide crystals with tailored facets. *Chem. Rev.* **2014**, *114*, 9559–9612. [CrossRef] [PubMed]
87. Liu, J.; Olds, D.; Peng, R.; Yu, L.; Foo, G.; Qian, S.; Keum, J.; Guiton, B.; Wu, Z.; Page, K. Quantitative analysis of the morphology of {101} and {001} faceted anatase TiO_2 nanocrystals and its implication on photocatalytic activity. *Chem. Mater.* **2017**, *29*, 5591–5604. [CrossRef]
88. Roy, N.; Sohn, Y.; Pradhan, D. Synergy of low-energy {101} and high-energy {001} TiO_2 crystal facets for enhanced photocatalysis. *ACS Nano* **2013**, *7*, 2532–2540. [CrossRef] [PubMed]
89. Li, C.; Koenigsmann, C.; Ding, W.; Rudshteyn, B.; Yang, K.; Regan, K.; Konezny, S.; Batista, V.; Brudvig, G.; Schmuttenmaer, C.; Kim, J.-H. Facet-dependent photoelectrochemical performance of TiO_2 nanostructures: An experimental and computational study. *J. Am. Chem. Soc.* **2015**, *137*, 1520–1529. [CrossRef] [PubMed]
90. Zhou, P.; Zhang, H.; Ji, H.; Ma, W.; Chen, C.; Zhao, J. Modulating the photocatalytic redox preferences between anatase TiO_2 {001} and {101} surfaces. *Chem. Commun.* **2017**, *53*, 787–790. [CrossRef] [PubMed]
91. Chamtouri, M.; Kenens, B.; Aubert, R.; Lu, G.; Inose, T.; Fujita, Y.; Masuhara, A.; Hofkens, J.; Uji-i, H. Facet-dependent diol-induced density of states of anatase TiO_2 crystal surface. *ACS Omega* **2017**, *2*, 4032–4038. [CrossRef] [PubMed]